

01 Jan 2004

New External Neuro-Controller for Series Capacitive Reactance Compensator in a Power Network

Jung-Wook Park

Ganesh K. Venayagamoorthy
Missouri University of Science and Technology

Ronald G. Harley

Follow this and additional works at: https://scholarsmine.mst.edu/ele_comeng_facwork



Part of the [Electrical and Computer Engineering Commons](#)

Recommended Citation

J. Park et al., "New External Neuro-Controller for Series Capacitive Reactance Compensator in a Power Network," *IEEE Transactions on Power Systems*, Institute of Electrical and Electronics Engineers (IEEE), Jan 2004.

The definitive version is available at <https://doi.org/10.1109/TPWRS.2004.826802>

This Article - Journal is brought to you for free and open access by Scholars' Mine. It has been accepted for inclusion in Electrical and Computer Engineering Faculty Research & Creative Works by an authorized administrator of Scholars' Mine. This work is protected by U. S. Copyright Law. Unauthorized use including reproduction for redistribution requires the permission of the copyright holder. For more information, please contact scholarsmine@mst.edu.

New External Neuro-Controller for Series Capacitive Reactance Compensator in a Power Network

Jung-Wook Park, *Member, IEEE*, Ronald G. Harley, *Fellow, IEEE*, and Ganesh K. Venayagamoorthy, *Senior Member, IEEE*

Abstract—The controllable capacitive reactance can be used as the input variable for the external controller of a series capacitive reactance compensator (SCRC) to improve the damping of low-frequency oscillations of the rotor angle and active power in a power system. Conventional linear PI controllers are tuned for best performance at one specific operating point of the nonlinear power system. At other operating point its performance degrades. Nonlinear optimal neuro-controllers are able to overcome this degradation. In this paper, the dual heuristic dynamic programming (DHP) optimization algorithm is applied to design an external nonlinear optimal neuro-controller for the SCRC. Simulation studies using PSCAD/EMTDC[®] software are presented.

Index Terms—Dual heuristic programming, flexible ac transmission systems devices, optimization, power system, series capacitive reactance compensator.

I. INTRODUCTION

It has long been recognized that the damping of power oscillations can be improved by dynamically altering the series impedance of one of the transmission lines in an interconnected power network using some form of controllable series capacitive compensator [1]. In the last decade, the *series* flexible ac transmission systems (FACTS) devices [2] have been progressively developed to deal with the above control objective.

For the series capacitive reactance compensator (SCRC) FACTS device, Ooi *et al.* [3], [4] first proposed making use of a stand-alone inverter both to maintain dc capacitor voltage of the inverter and to ensure the series reactance condition at the inverter's ac terminals. Rigby and Harley *et al.* [5] extended the original work proposed by Ooi *et al.* into a working laboratory prototype of a SCRC, and improving the performance of the original SCRC scheme by modifying the voltage regulator structure. Based on this work, they also reported [6] on the analysis of a power oscillation damping scheme by applying an *external linear-controller* with the aid of properly designed

supplementary controls [7] to the SCRC, and they also considered the impact of the SCRC's own internal dynamics on the performance of an external damping controller. It is important to note that the study of the *external control* (called secondary or functional operation control [2]) for the FACTS device makes it possible to progress further toward hierarchical control and possible global dynamic optimization in large-scale power networks.

In this paper, the theory and operation of the SCRC (in [5]) as well as its conventional external linear-controller (CONVEC) (in [6]) are briefly described. Thereafter, the new external optimal neuro-controller for the SCRC using the dual heuristic programming (DHP) optimization algorithm [8], [9] is designed as an alternative to the CONVEC in order to improve the damping of low frequency active power oscillations.

II. ANALYSIS OF A DAMPING SCHEME FOR SCRC

Based on the work proposed in [5] and [6], this section briefly summarizes the operation of the internal and external control schemes for the SCRC in Fig. 1, which shows a single generator (160 MVA, 15 kV (L-L)) connected to an infinite bus through two transmission lines, labeled Line #1 and Line #2. The parameters of the synchronous generator in Fig. 1 are given in [10].

Also, the EXAC1A (IEEE alternator supplied rectifier excitation systems) and H_TUR1/GOV1 (IEEE type hydro turbine-governor) models in PSCAD/EMTDC software library [11] are used as the AVR/exciter and turbine/governor systems, respectively.

A. Internal Control of the SCRC

The internal control scheme for the SCRC is shown in Fig. 2. The main objectives of the inner control for the SCRC are:

- to ensure that the injected voltage at the ac terminals of the inverter is in quadrature with the transmission line current. In other words, the injected voltage v_c in Fig. 1 lags the line current i_s by 90° such that the injected voltage appears to be a capacitive volt drop (as shown in Fig. 3).
- to keep the voltage V_{dc} constant during steady state, like other series FACTS devices including the static synchronous series compensator (SSSC) [8] (as shown in Fig. 4).

For the operation of the SCRC, the transmission line currents i_{sa} , i_{sb} , and i_{sc} are first transformed by Park's transformation into d and q axes components i_d and i_q in a synchronously rotating reference frame. Then, the peak value of the current vector $\sqrt{i_d^2 + i_q^2}$ is calculated.

Manuscript received October 22, 2003. This work was supported in part by the National Science Foundation (NSF) under Grant ECS-0231632 and in part by the Duke Power Company, Charlotte, NC. and was completed while the first author was affiliated with Georgia Institute of Technology, Atlanta, GA.

J.-W. Park was with the Georgia Institute of Technology, Atlanta, GA 30332-0250 USA. He is now with the Department of Electrical and Computer Engineering, University of Wisconsin-Madison, Madison, WI 53706-1691 USA (e-mail: jungwookpark@ieee.org).

R. G. Harley is with the School of Electrical and Computer Engineering, Georgia Institute of Technology, Atlanta, GA 30332-0250 USA (e-mail: rharley@ece.gatech.edu).

G. K. Venayagamoorthy is with the Department of Electrical and Computer Engineering, University of Missouri-Rolla, Rolla, MO 65409-0249 USA (e-mail: ganeshv@ece.umr.edu).

Digital Object Identifier 10.1109/TPWRS.2004.826802

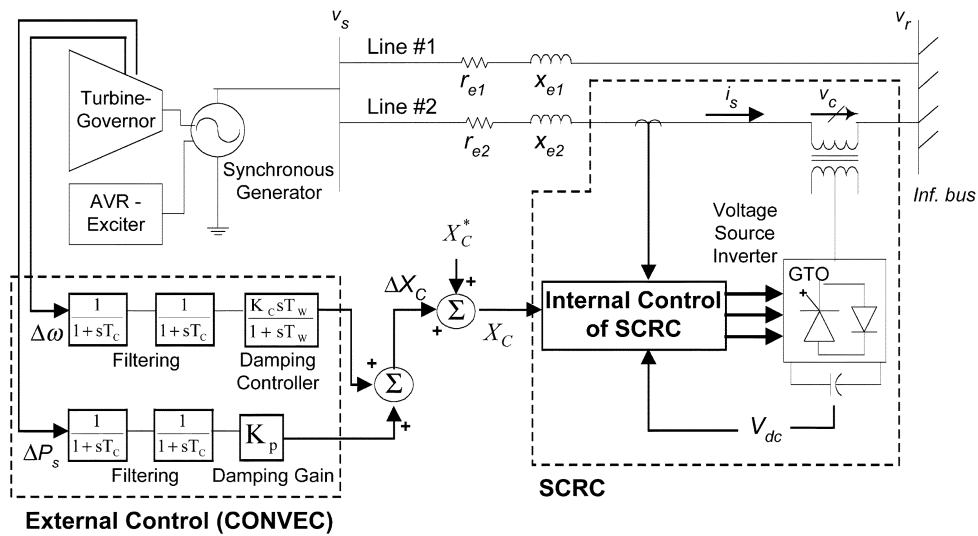


Fig. 1. Schematic single-line diagram showing an inverter-based controllable series capacitive reactive compensator with external controller.

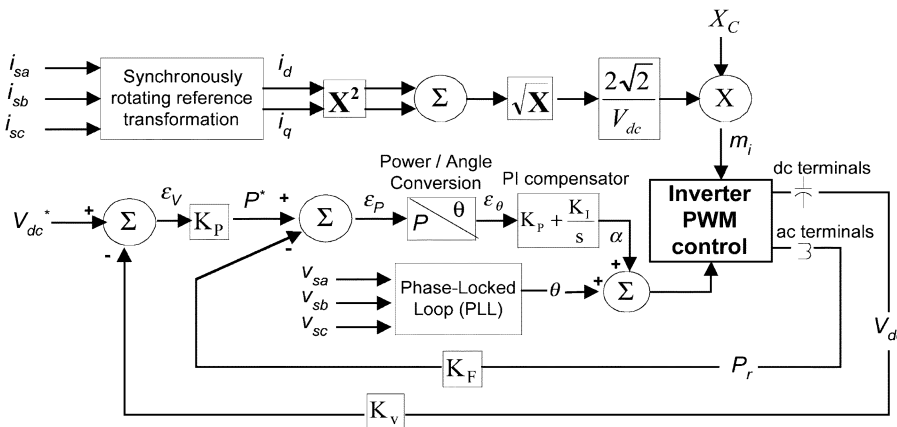
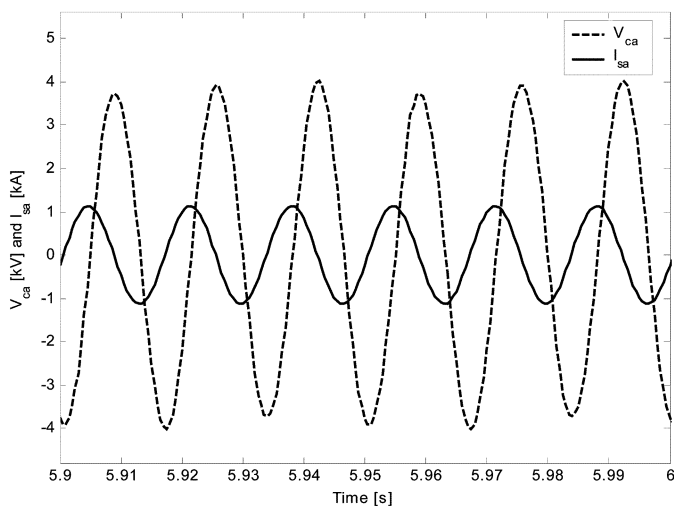


Fig. 2. Internal control scheme of the SCRC.


 Fig. 3. Injected voltage v_{ca} and line current i_{sa} at steady state ($t = 5.9$ to 6 s).

The desired magnitude $|v_{c,pk}|$ of the compensating voltage vector is now determined by multiplying the magnitude of the

current vector $\sqrt{i_d^2 + i_q^2}$ by the factor $2\sqrt{2}/V_{dc}$ and the total commanded value of capacitive reactance X_C , and the result is the modulation index m_i for the sinusoidal PWM inverter.

Also, the structure of the SCRC in Fig. 2 has an inner power control loop as well as an outer voltage control loop. The dc capacitor voltage V_{dc} is fed back and subtracted from the reference value V_{dc}^* to form the voltage error ϵ_V in the outer loop, which is used to produce the commanded power P^* . The action of the SCRC in maintaining a constant voltage V_{dc} at steady state ensures that no real power is exchanged between the inverter and the transmission line, thereby ensuring that the line current leads the injected voltage by 90°.

Meanwhile, the instantaneous real power P_r at the ac terminals of the inverter is fed back and subtracted from the commanded power P^* to form the error ϵ_P for the inner loop, which is thereafter converted to the commanded phase angle α for the PWM inverter after passing through the power/angle conversion block and PI compensator.

The advantage gained by the inclusion of the inner loop is that the necessary bandwidth of the phase-locked loop (PLL) can be

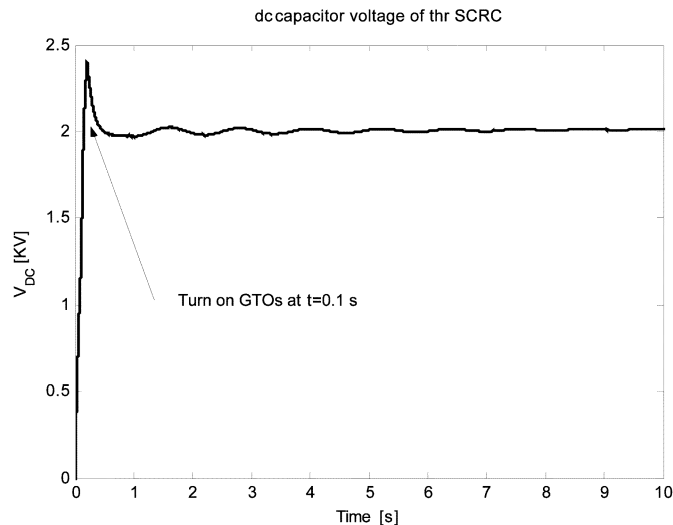


Fig. 4. DC capacitor voltage of the SCRC at steady state ($t = 0$ to 10 s).

achieved with less compromise in the response of the system to a disturbance on the dc side of the inverter [5].

B. Conventional External Control of SCRC

The objective of the conventional external linear-controller (CONVEC) for the SCRC (dashed block in Fig. 1) is to improve the system damping performance.

By the internal control described in the previous subsection, the voltage v_c injected by the SCRC to the transmission line appears to be a volt drop across a capacitive reactance $-jX_C^* = v_c/i_s$ (see Fig. 3), of which the magnitude or set-point X_C^* can be specified.

Under a steady state condition with no power swings, $\Delta\omega$ (speed deviation) and ΔP_S (active power deviation) at generator terminal are zero, therefore the supplementary control signal ΔX_C is zero, and $X_C^* = X_C$. Otherwise, X_C^* is modulated by ΔX_C to provide damping.

From a system perspective, there are two design and performance issues;

- 1) The CONVEC should be able to command proper changes in compensating reactance X_C in order to damp low frequency active power oscillations that occur between the generator and transmission system.
- 2) The internal control of the SCRC should be able to respond to the commands from the CONVEC.

For issue (1), it is necessary to briefly review the analytical approach to see the impact of dynamic changes in series compensating reactance on the damping of a synchronous generator. It is reported in [7] that the speed deviation $\Delta\omega$ of a generator can be used to generate the supplementary control signal ΔX_C (in Fig. 1) from the external control. The design of the CONVEC in Fig. 1 is based on the work in [7].

In this paper, the active power deviation signal ΔP_S is also considered as the input of the CONVEC. The use of additional variable ΔP_S can provide the external controller more damping, compared to in case that only the $\Delta\omega$ is used as the input of an external controller. This is shown in Section IV.A by simulation result.

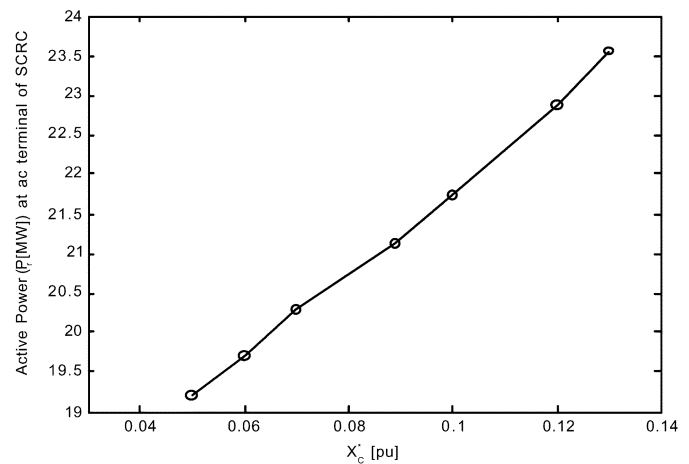


Fig. 5. Active power (P_r) at the ac terminal of SCRC versus X_C^* .

In Fig. 1, the SCRC is connected to Line #2, and provides a set-point value of capacitive reactance compensation of $X_C^* = -j0.089$ pu during a steady state condition. The deviation signals $\Delta\omega$ and ΔP_S from the synchronous generator are passed through the CONVEC (two first-order low-pass filters, damping controller with a proportional gain K_C and a washout filter for $\Delta\omega$, and a gain damping K_P for ΔP_S) to form the signal ΔX_C . Then, ΔX_C is added to X_C^* resulting in the total commanded value of compensating reactance X_C at the input for the internal control of the SCRC. A more detailed explanation of how to design two first-order low-pass filters (with cut-off frequency of 13 Hz) and a damping controller are described in [6].

The selection of the proportional damping gain K_C and K_P (in Fig. 1) is determined by evaluating the damping of oscillations after a severe fault like a three phase short circuit (also, see [6]). In this paper, the value of $K_C = 1.5$ and $K_P = 0.02$ (which are designed at a particular operating condition) are used for several case studies in Section IV.

For issue (2), the result in Fig. 5 shows that the relationship between the value of X_C^* and active power P_r at the ac terminal of the SCRC appears to be almost linear. This characteristic enables the CONVEC to be an effective external controller such that the internal control of the SCRC is able to respond directly to the commands from the CONVEC. However, the X_C^* within ± 0.04 pu around the set-point value of $-j0.089$ pu is used. These specified boundary values (0.13 pu at maximum and 0.05 pu at minimum) are chosen to correspond to the range of the value of X_C^* , for which the practical series compensator has already been tested under a steady state condition in [6].

III. NEW EXTERNAL OPTIMAL NEURO-CONTROLLER DESIGN

This section proposes a new external nonlinear optimal neuro-controller using the dual heuristic programming (DHP) algorithm to replace the CONVEC shown in Fig. 1. This is illustrated in Fig. 6. The external neuro-controller will be shown to have the better damping performance than the CONVEC.

A detailed comparison of two adaptive critic designs (ACDs) were carried out in [17] and the DHP algorithm was shown to be the most powerful of the two. Therefore the DHP algorithm is

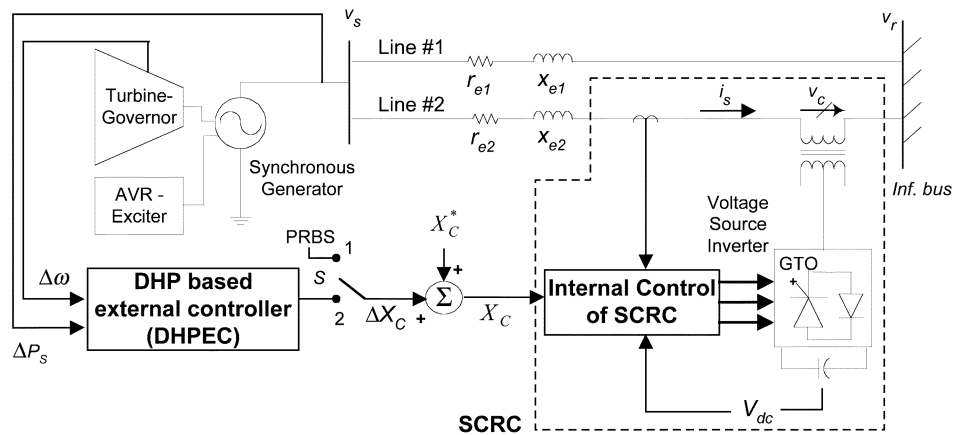


Fig. 6. Schematic single-line diagram showing the new DHP based external optimal neuro-controller (DHPEC).

selected for this study. This algorithm solves the infinite horizon optimal control problem based on the neuro-dynamic programming (NDP) approach using artificial neural networks (ANN's) [12] (by the estimating the derivatives of optimal cost-to-go function J with respect to states of the plant). A more detailed background of the ACDs and their relation to classical optimal control theory is given in [12].

The design of the new DHP based external optimal neuro-controller (DHPEC) requires a model network, a critic network, and an action network for its implementation [8], [9]. In the following subsections, descriptions of how to design the model, critic, and action networks, using the multilayer perceptron neural network (MLPNN) [13], are given.

A. Design of the Model Network

The design of the model network (identifier) is an important part in the implementation of the model-dependent ACDs because its capability to learn the dynamics of the plant directly affects the performance of the critic and action networks. The input-output mapping structure of the model network for the DHPEC to replace the CONVEC, is shown in Fig. 7. The structure of the model neural network is based on the nonlinear autoregressive moving average with exogenous inputs (NARMAX) model. Three variables are used for its input, which are the real power deviation at the generator terminals (ΔP_S), speed deviation ($\Delta\omega$), and output control signal from the action network (ΔX_C). This assumes that ΔP_S and $\Delta\omega$ will be available to the DHPEC at any remote location.

The three time-lagged values of $t-1$, $t-2$, and $t-3$ for the inputs of the model network are used, and this tapped time delay of order 3 is enough to have an acceptable tracking capability of nonlinear dynamics in a power plant (as reported in [8], [12], and [13]) when the model network is trained by the backpropagation algorithm [13].

It is important to note that, as the CONVEC shown in Fig. 1, the variable ΔP_S is added for the design of the DHPNC because it can provide the model network with additional information about the dynamics of the plant. In other words, the proposed DHPNC can easily deal with variations of active power at the generator terminals (or any other number of input variables). Moreover, this design could be useful for the study of the global

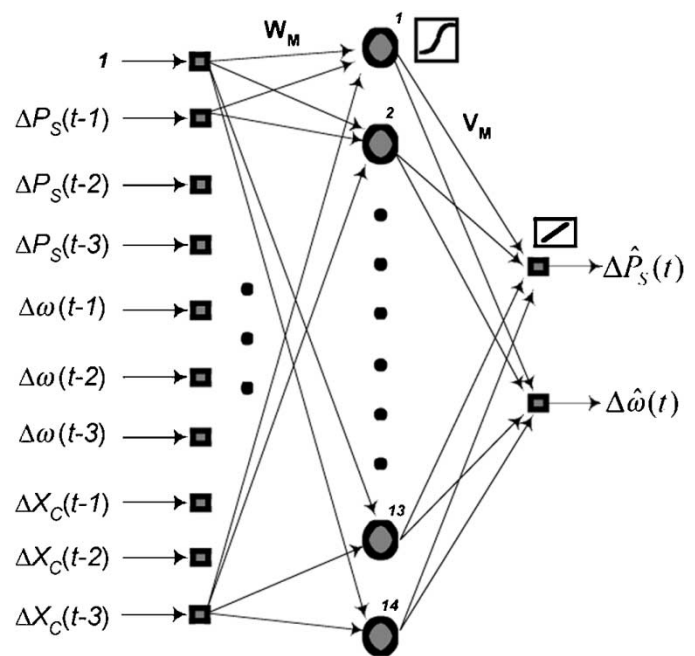


Fig. 7. Input-output mapping of the model network for the external DHP controller.

dynamic optimization to reduce the total energy loss (in case of minimizing the active power deviation at every generator terminals) in a practical multi-machine power system network [14]. Fourteen neurons in the hidden layer are chosen after evaluating convergence properties as reported in [13].

A more detailed explanation of how to design/train the model network is given in [14].

B. Critic and Action Networks

After training the model network, the critic and action networks are designed as reported in [8] and [9]. The input-output mapping structures for the critic and action networks are shown in Figs. 8 and 9, respectively.

Ten neurons in the hidden layer are used for both the critic and action networks. The inputs of the critic network are the outputs ($\Delta\hat{Y}(t) = [\Delta\hat{P}_S(t), \Delta\hat{\omega}(t)]$) from the model network

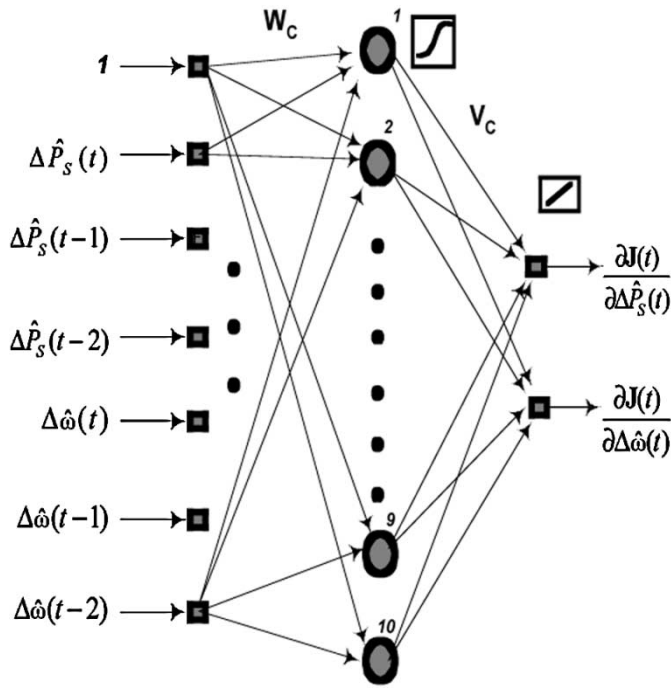


Fig. 8. Input-output mapping of the critic network for the DHPEC.

and their two time-delayed values; the outputs of the critic network are the derivatives of function \mathbf{J} with respect to the observables of the state (by the model network), which are $\lambda(t) = \partial \mathbf{J}(t) / \partial \Delta \hat{\mathbf{Y}}(t) = [\partial \mathbf{J}(t) / \partial \Delta \hat{P}_S(t), \partial \mathbf{J}(t) / \partial \Delta \hat{\omega}(t)]$.

For the design of the action network, the following two different action networks are tested;

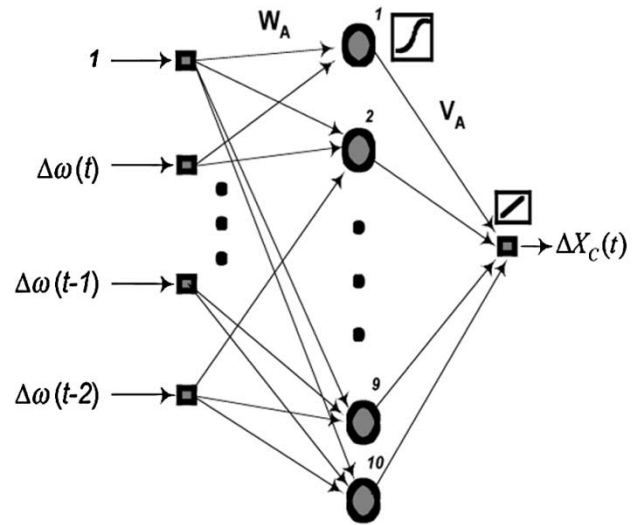
- The action network with only one input variable $\Delta \omega(t)$ and its two time-delayed values [see Fig. 9(a)] for its inputs.
- The action network with two input variables $(\Delta P_S(t), \Delta \omega(t))$ and their two time-delayed values [see Fig. 9(b)].

For both the above cases, the output of the action networks is the same $\mathbf{A}(t) = \Delta X_C(t)$ as in the CONVEC. From Fig. 9(b), the availability of the variable ΔP_S (which is used to give the model network more information about the dynamics of the plant) can also make it possible to affect the neuro-controller's dynamic performance, compared to the action network with only one input variable $\Delta \omega$ shown in Fig. 9(a). The result showing the control performances by these two action networks is given in the next Section IV.A.

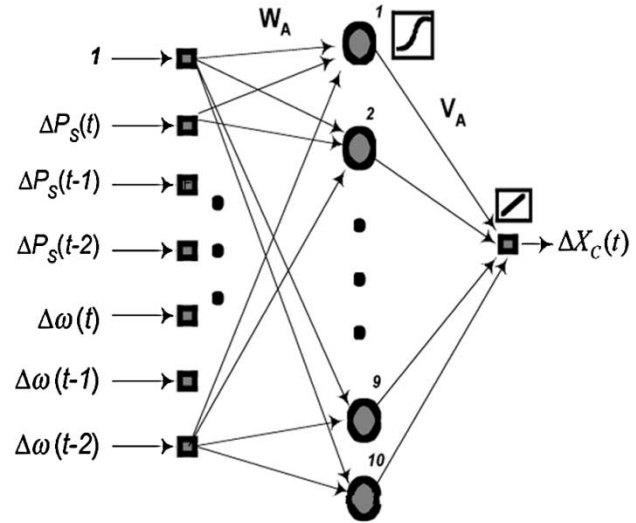
The weights of the critic network are updated by the configuration (to minimize the error vector $\mathbf{e}_C(t)$) shown in Fig. 10, and the associated mathematical equations are given in below [8]:

$$\|E_C\| = \sum_t \mathbf{e}_C^T(t) \mathbf{e}_C(t), \quad (1)$$

$$\mathbf{e}_C(t) = \frac{\partial \mathbf{J}[\Delta \hat{\mathbf{Y}}(t)]}{\partial \Delta \hat{\mathbf{Y}}(t)} - \gamma \frac{\partial \hat{\mathbf{J}}[\Delta \hat{\mathbf{Y}}(t+1)]}{\partial \Delta \mathbf{Y}(t)} - \frac{\partial U[\Delta \mathbf{Y}(t)]}{\partial \Delta \mathbf{Y}(t)}. \quad (2)$$



(a) Action network with one input variable ($\Delta \omega$).



(b) Action network with two input variables (ΔP_S and $\Delta \omega$).

Fig. 9. Input-output mapping of the action network for the DHPEC.

The second term (for the j th component) of right-hand side in (2) can be expressed as follow:

$$\frac{\partial \hat{\mathbf{J}}[\Delta \hat{\mathbf{Y}}(t+1)]}{\partial \Delta \mathbf{Y}_j(t)} = \sum_{i=1}^n \hat{\lambda}_i(t+1) \frac{\partial \hat{\mathbf{Y}}_i(t+1)}{\partial \Delta \mathbf{Y}_j(t)} + \sum_{k=1}^m \sum_{i=1}^n \hat{\lambda}_i(t+1) \frac{\partial \Delta \hat{\mathbf{Y}}_i(t+1)}{\partial \mathbf{A}_k(t)} \frac{\partial \mathbf{A}_k(t)}{\partial \Delta \mathbf{Y}_j(t)}, \quad (3)$$

where n and m are the numbers of outputs of the model and the action networks, respectively. Using (3), each component of the error vector $\mathbf{e}_C(t)$ from (2) is computed by

$$\mathbf{e}_{Cj}(t) = \frac{\partial \mathbf{J}[\Delta \hat{\mathbf{Y}}(t)]}{\partial \Delta \mathbf{Y}_j(t)} - \gamma \frac{\partial \hat{\mathbf{J}}[\Delta \hat{\mathbf{Y}}(t+1)]}{\partial \Delta \mathbf{Y}_j(t)} - \frac{\partial U[\Delta \mathbf{Y}(t)]}{\partial \Delta \mathbf{Y}_j(t)} - \sum_{k=1}^m \frac{\partial U[\Delta \mathbf{Y}(t)]}{\partial \mathbf{A}_k(t)} \frac{\partial \mathbf{A}_k(t)}{\partial \Delta \mathbf{Y}_j(t)}. \quad (4)$$

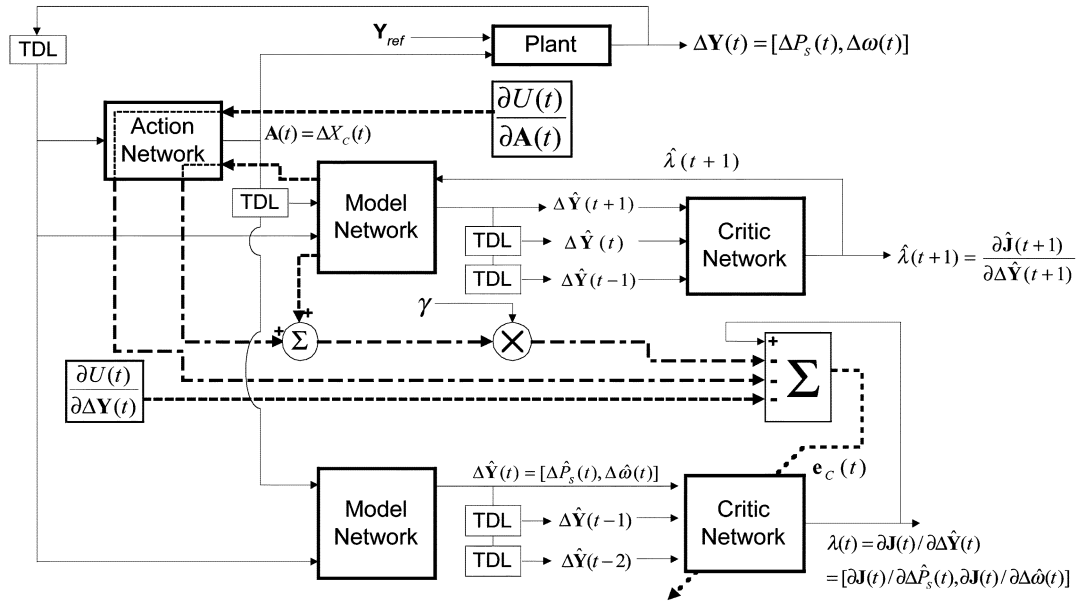


Fig. 10. Critic network adaptation in DHP: This diagram shows the implementation of (4). The same critic network is shown for two consecutive times, t and $t + 1$. The discount factor γ is chosen to be 0.5. Backpropagation paths are shown by dotted and dash-dot lines. The output of the critic network $\lambda(t + 1)$ is backpropagated through the model network from its outputs to its inputs, yielding the first term of (3) and $\partial\mathbf{J}(t + 1)/\partial\mathbf{A}(t)$. The latter is backpropagated through the action network from its outputs to its inputs forming the second term of (3). Backpropagation of the vector $\partial U(t)/\partial\mathbf{A}(t)$ through the action network results in a vector with components computed as the last term of (4). The summation of all these signals produces the error vector $\mathbf{e}_c(t)$ used for training the critic network.

Using (4), the weights for the critic network are incrementally updated by the following equation:

$$\Delta\mathbf{W}_C(t) = -\eta_C \mathbf{e}_C^T(t) \frac{\partial \mathbf{e}_C(t)}{\partial \mathbf{W}_C(t)}, \quad (5)$$

where η_C is a positive learning rate ($=0.02$).

The adaptation of the action network is illustrated in Fig. 11, which propagates $\hat{\lambda}(t + 1)$ back through the model network to the action network. The goal of this adaptation is expressed in (6), and then the weights of the action network are updated by (7).

$$\frac{\partial U[\Delta\mathbf{Y}(t)]}{\partial \mathbf{A}(t)} + \gamma \frac{\partial \hat{\mathbf{J}}[\Delta\hat{\mathbf{Y}}(t + 1)]}{\partial \mathbf{A}(t)} = 0 \quad \forall t. \quad (6)$$

$$\Delta\mathbf{V}_A(t) = -\eta_A \left[\frac{\partial U[\Delta\mathbf{Y}(t)]}{\partial \mathbf{A}(t)} + \gamma \frac{\partial \hat{\mathbf{J}}[\Delta\hat{\mathbf{Y}}(t + 1)]}{\partial \mathbf{A}(t)} \right]^T \frac{\partial \mathbf{A}(t)}{\partial \mathbf{V}_A(t)} \quad (7)$$

where η_A is a positive learning rate ($=0.02$).

C. Derivation of Utility Function

The discount factor γ of 0.5 is used in (2) and (6), and the utility function $U(t)$ in (8) is used during training of the critic and action networks.

$$U(t) = [0.1\Delta P_S(t) + 0.1\Delta P_S(t - 1) + 0.1\Delta P_S(t - 2)]^2 + [\Delta\omega(t) + \Delta\omega(t - 1) + 0.01\Delta\omega(t - 2)]^2 \quad (8)$$

A detailed explanation for the derivation of the utility function in (8) is given in [9]. This utility function plays an important role to form the user-defined optimal cost-to-go function \mathbf{J} , and is selected to give the best trade-off between *performance*

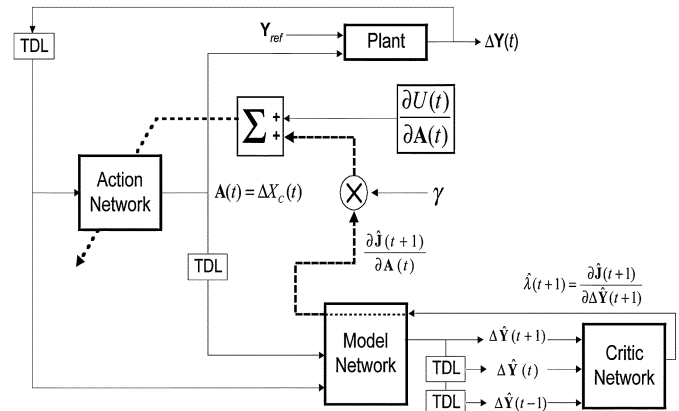


Fig. 11. Action network adaptation in DHP: The discount factor γ is chosen to be 0.5. Backpropagation paths are shown by dotted lines. The output of the critic network $\hat{\lambda}(t + 1)$ at time $(t + 1)$ is backpropagated through the model network from its outputs to its inputs (output of the action network), and the resulting vector multiplied by the discount factor ($\gamma = 0.5$) and added to $\partial U(t)/\partial\mathbf{A}(t)$. Then, an incremental adaptation of the action network is carried out by (6) and (7).

and *cost of control*. The utility function has to be positive and a quadratic form is therefore selected.

D. Overall Training Procedure

A detailed explanation about the training procedures for a model, a critic, and an action network in the DHP algorithm are described in [8] and [9]. Note that the training procedure to implement the DHP algorithm consists of two training cycles: one for the model network and the other for the critic/action networks. This is illustrated in Fig. 12.

The model network is first trained to learn the dynamics of the plant before the critic and action networks are trained. After the weights of the model network have converged (identifying

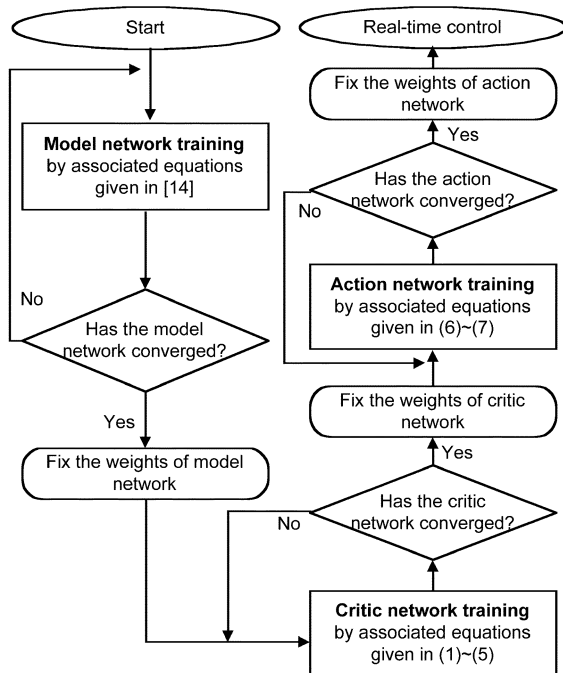


Fig. 12. Training procedure for the model, critic, and action networks.

the plant outputs accurately as shown in [14]), they are fixed. Then, the critic network is trained by associated (1)–(5) until the derivatives of $\mathbf{J}(\lambda(t))$ in Fig. 10) have converged to the value as small as possible (this is so-called the *value iteration* by the critic network). Then, the weights of the critic network are fixed. Finally, the action network is trained by associated (6) and (7) until the value of left-hand side in (6) has converged to zero (this is so-called the *policy iteration* by the action network). Thereafter the weights of the action network are fixed. The fixed weights of the critic and action networks are now ready to be used in a real-time control operation.

This training takes place *at the same particular operating point* as used for tuning of the CONVEC parameters. The pseudo-random binary signals (PRBS's) [9], [14] are injected for training the model network with the switch S in position 1 in Fig. 6. For the training of the critic and action networks, the switch S is in position 2. Typical PRBS's values of ΔX_C appear in Fig. 13.

E. Computing Requirement

The computing time needed to train all the networks in Fig. 12 varies and depends on the particular system, rate of convergence, and computer processor speed. For the case study in Section IV, it took 24 hours for the critic network (with $\eta_C = 0.02$) and 12 hours for the action network (with $\eta_A = 0.02$) to converge on a Window NT workstation (with Intel Pentium-III) during training by PSCAD/EMTDC® software. Research is continuing to reduce these times.

IV. CASE STUDIES IN SINGLE MACHINE INFINITE BUS SYSTEM

After training the model network, the critic and action networks are trained until their acceptable performances are accomplished; thereafter the parameters (weights) of the critic

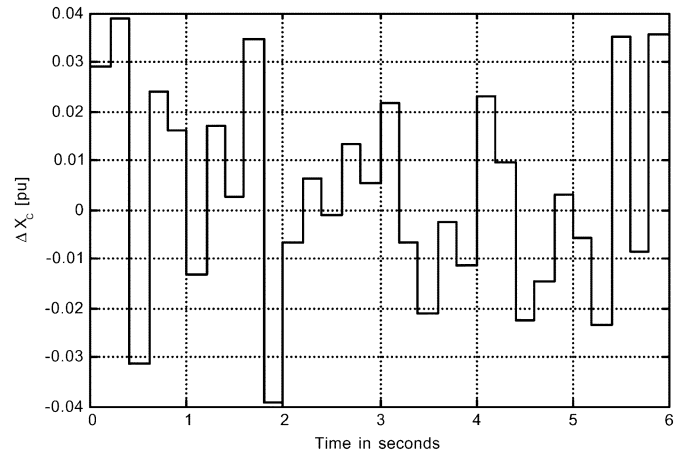


Fig. 13. Pseudo random binary signals used for ΔX_C during training.

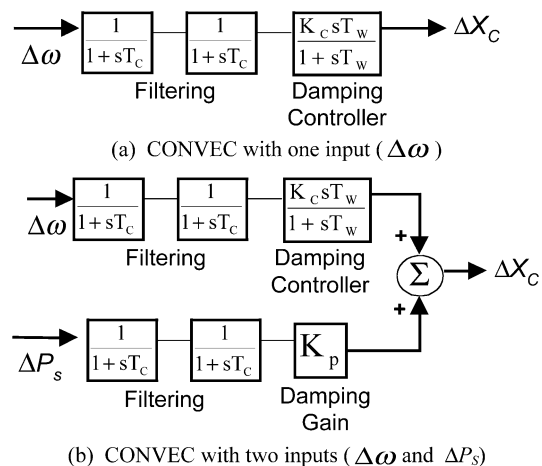


Fig. 14. CONVEC with one input and with two inputs.

and action networks for the DHPEC are fixed and then used for real-time simulation tests in the single machine infinite bus (SMIB) system shown in Figs. 1 and 6.

The control performances by the action networks (of the DHPEC) with one input variable [in Fig. 9(a)] and with two input variables [in Fig. 9(b)] are firstly compared. The damping performances of the CONVEC (in Fig. 1) with one input ($\Delta\omega$) and with two inputs ($\Delta\omega$ and ΔP_S) are also compared. This is illustrated in Fig. 14.

Then, the dynamic damping performances of the SCRC with a fixed set-point value of X_C^* is firstly evaluated without an external controller, then with the CONVEC in Fig. 1 (with $K_C = 1.5$ and $K_P = 0.02$), and then with the DHPEC in Fig. 6. The dynamic damping performances of the controllers are evaluated at two different operating points by a 100 ms three phase short circuit applied at the infinite bus.

A. Tests at the Operating Condition Where Controllers Have Been Designed

1) *Controllers With One Input/Two Input Variables:* The control performances of the two action networks (in Fig. 9) and two CONVEC's (in Fig. 14) with one input variable ($\Delta\omega$) and two input variables ($\Delta\omega$ and ΔP_S) are now evaluated by a 100 ms three phase short circuit applied to the infinite bus (in

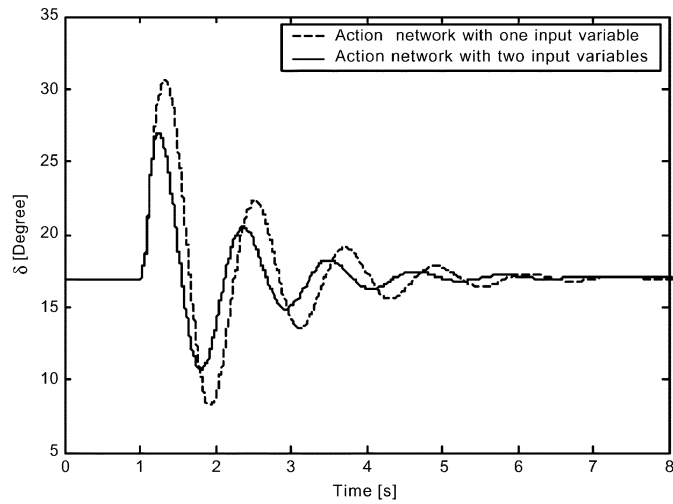


Fig. 15. A 100 ms three phase short circuit test for the DHPEC: δ [°].

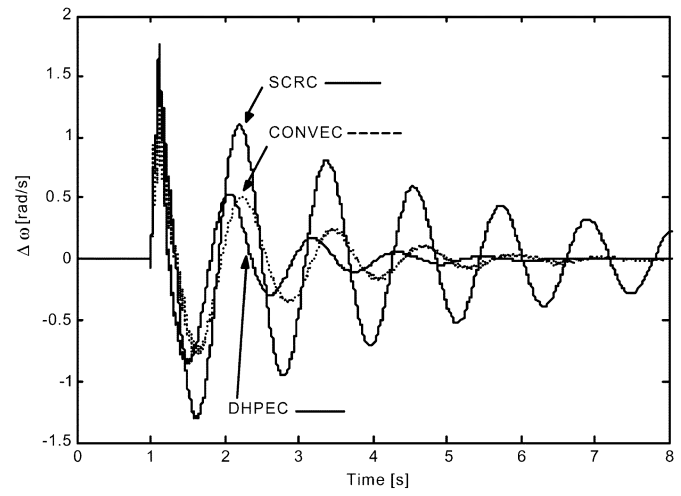


Fig. 18. A 100 ms three phase short circuit test: $\Delta\omega$ [rad/s].

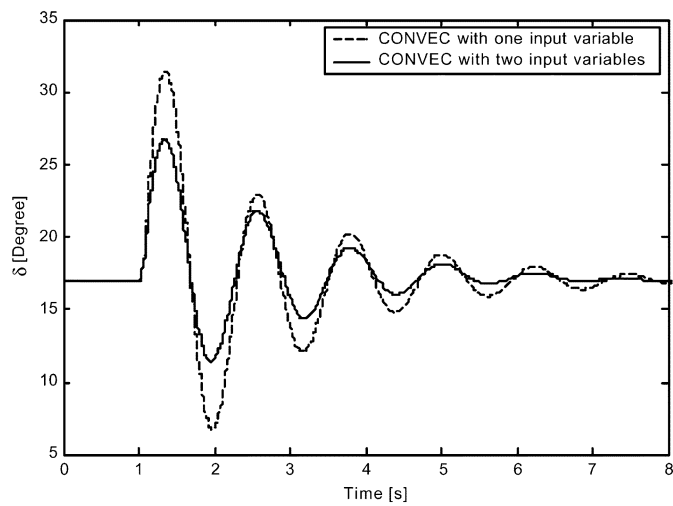


Fig. 16. A 100 ms three phase short circuit test for the CONVEC: δ [°].

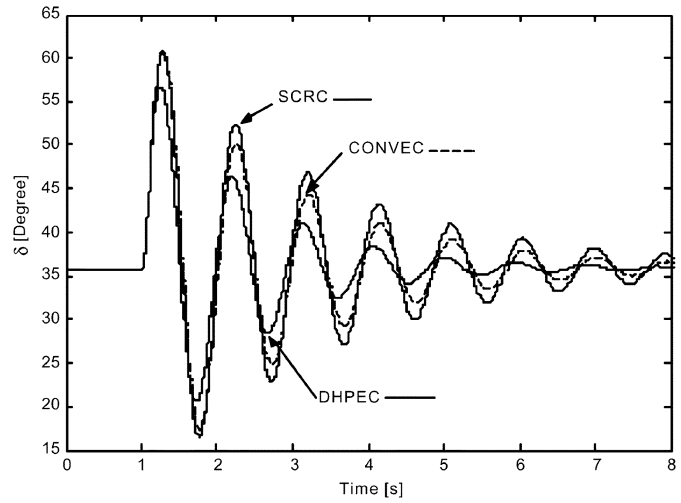


Fig. 19. A 100 ms three phase short circuit test at OP-II: δ [°].

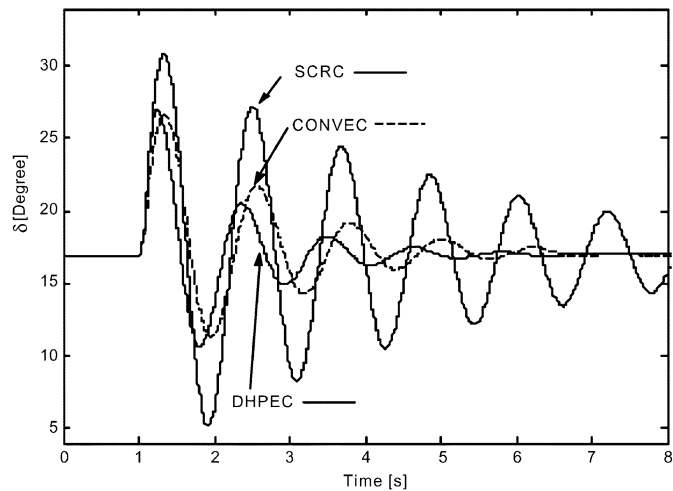


Fig. 17. A 100 ms three phase short circuit test: δ [°].

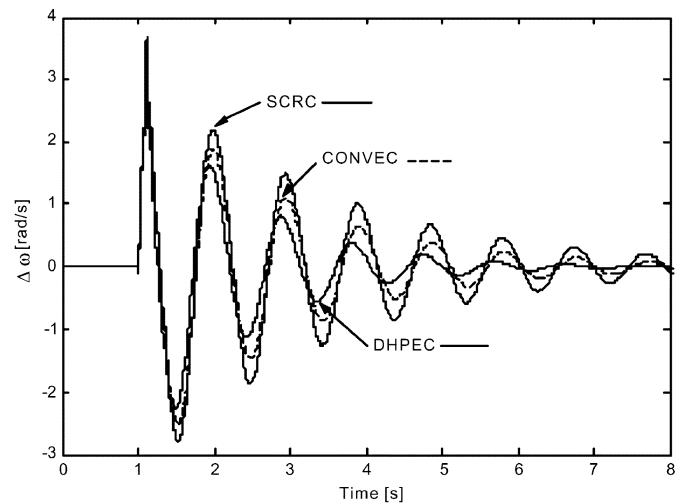


Fig. 20. A 100 ms three phase short circuit test at OP-II: $\Delta\omega$ [rad/s].

Figs. 1 and 6) at $t = 1$ s, at a particular operating condition (called OP-I) where the DHPEC was trained and the CONVEC was tuned. In other words, the generator operates with a rotor

angle of 16.9° ($P_t = 0.25$ pu, $Q_t = 0.16$ pu) at a pre-fault steady state operating point (OP-I), where the same amount of power is flowing in Line #1 and Line #2 (with the same line impedances).

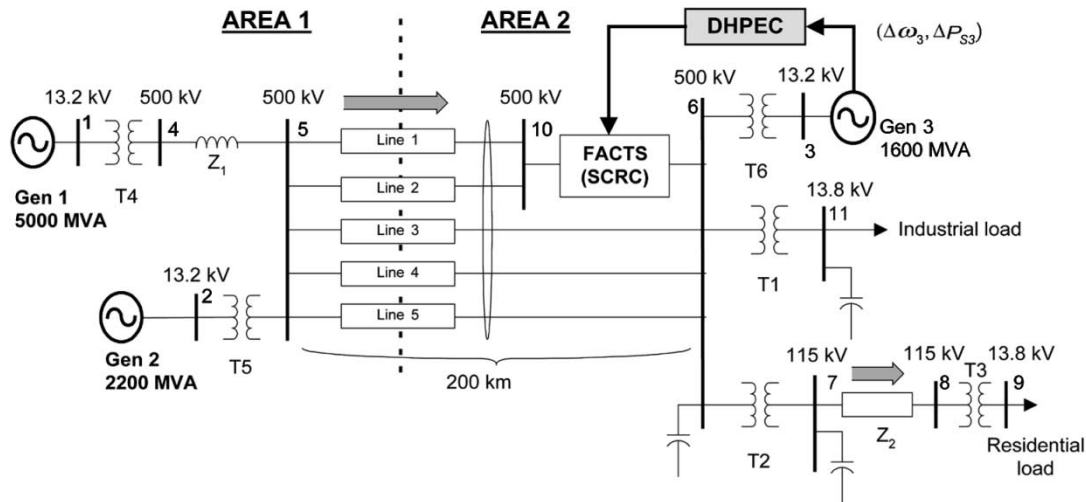


Fig. 21. Large-scale multi-machine power system equipped with SCRC.

The results are shown in Figs. 15 and 16. From Fig. 15, it is clearly shown that the action network with two input variables ($\Delta\omega$ and ΔP_S) has a better damping performance than the action network with only one input variable ($\Delta\omega$).

Likewise, it is shown in Fig. 16 that the CONVEC with two input variables ($\Delta\omega$ and ΔP_S) improves the damping performance for low frequency oscillations more effectively than the CONVEC with one input ($\Delta\omega$). Therefore, the DHPEC [by the action network in Fig. 9(b)] and CONVEC [in Fig. 14(b)] with two input variables are used for further comparisons in the following subsections.

2) *Three Phase Short Circuit at Infinite Bus:* The controllers (DHPEC and CONVEC with two input variables) are now compared by the same 100 ms three phase short circuit test as used in the previous test at the operating condition, OP-I.

The results appear in Figs. 17 and 18 for the rotor angle (δ [°]) and speed deviation ($\Delta\omega$ [rad/s]), respectively. The curve SCRC indicates the response of system with only an internal controller (of the SCRC) and no external controller.

Figs. 17 and 18 clearly show that the damping control for low frequency power swings by the DHPEC is better after the first swing at the post-fault condition than those of the CONVEC and the SCRC.

B. Dynamic Performances at a Different Operating Condition

1) *Three Phase Short Circuit at Infinite Bus:* The control performances of the controllers are now re-tested at a different operating condition (called OP-II) from the above the OP-I. In other words, the line impedance (Z_{e1}) of the Line #1 in Figs. 1 and 6 is changed from $Z_{e1} = 0.04 + j0.75$ pu to $0.04 + j0.15$ pu, therefore, the amount of steady state active power flowing through the Line #1 is greater than that flowing through the Line #2. The generator is operating with a pre-fault rotor angle of 35.88° ($P_t = 0.56$ pu, $Q_t = 0.24$ pu). However, the parameters of the controllers are the same as those used in the previous subsection and have therefore not been tuned (CONVEC)/trained (DHPEC) for this new operating point.

The same 100 ms three phase short circuit as used in the previous test, is applied (as large disturbance) at the infinite

bus. The results appear in Figs. 19 and 20. They clearly show that the DHPEC still has the better damping performance at the post-fault condition than the SCRC and CONVEC, and the CONVEC is also more effective compared to the SCRC.

Differently from the results in Figs. 17 and 18, the DHPEC (in Figs. 19 and 20) shows the better damping than the CONVEC even in the first swing after the fault is applied. This proves that the performance of the CONVEC is degraded at the different operating point (OP-II) at which it was not tuned, compared to that of DHPEC with the same parameters as trained in the OP-I.

V. CASE STUDIES IN A MULTI-MACHINE POWER SYSTEM

The feasibility of the DHPEC on the multi-machine power system shown in Fig. 21 is now evaluated. This model has been used for the study of voltage stability on a practical large-scale power system in [15] and [16]. In Fig. 21, the sending end (in AREA1) has two generators (Gen 1 and Gen 2) transmitting power to the receiving area (AREA 2) through five 500 kV, 200 km long, transmission lines. Gen 1 is given a large inertia so that it functions as the slack bus. However, it is relatively small electrically (5000 MVA) in order to provide only limited voltage support (or reactive power support) for the load area in AREA 2. The parameters of Gen 2 and Gen 3 are identical and given in the Appendix D (Unit F18) of [10]. Also, Gen 1 and Gen 2 are equipped with an automatic voltage regulator (AVR)/exciter and a turbine/speed governor (GOV) system.

It is important to assume that Gen 3 is close enough to the SCRC FACTS device to be able to get the speed deviation and active power deviation signals to the controller (DHPEC) without any time delay.

The design and training procedure of the DHPEC on the multi-machine power system in Fig. 21 is the same as mentioned in the single machine system study. As in that case, the performances of the DHPEC are now evaluated by applying a large impulse type disturbance, a 300 ms three phase short circuit to bus 10 (in Fig. 21), at $t = 0.5$ s. The Gen 2 and Gen 3 are operating with rotor angles of 50.41° and 51.2° with respect to the bus 2 and 3 respectively during the pre-fault steady state operating point.

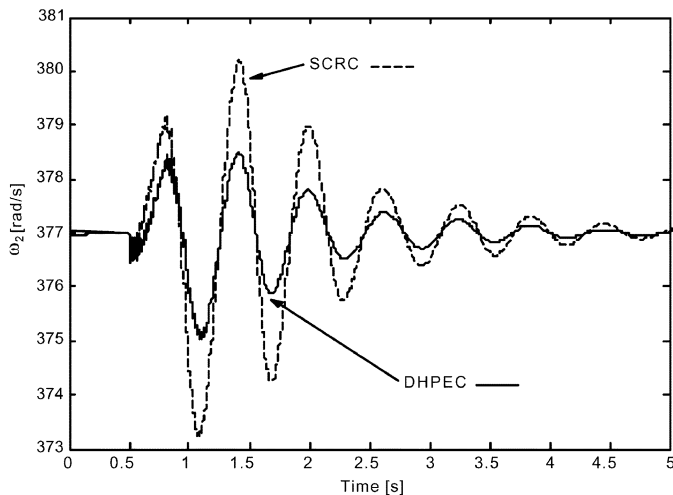


Fig. 22. A 300 ms three phase short circuit test at bus 10: ω_2 [rad/s].

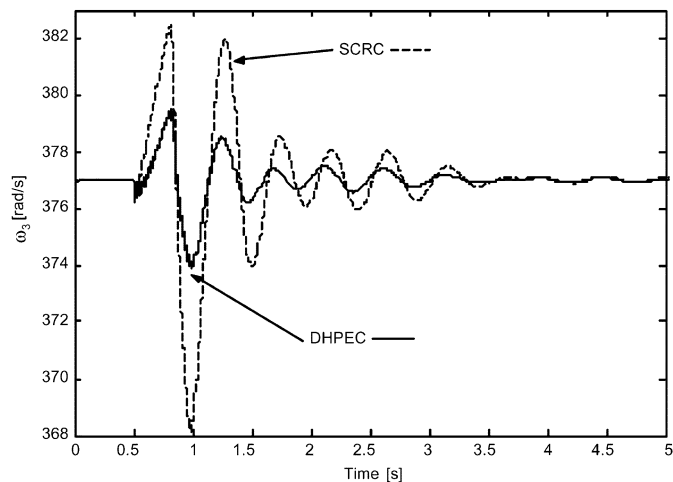


Fig. 23. A 300 ms three phase short circuit test at bus 10: ω_3 [rad/s].

The results are shown in Figs. 22 and 23 for the speeds (ω_2 and ω_3) of Gen 2 and Gen 3. They clearly show that the DHPEC still improves damping of low frequency oscillations more effectively, compared to the SCRC (without an external controller).

The further simulation results tested at a very different operating condition (at which the DHPEC was not trained) show that the DHPEC is still successful in damping of low frequency oscillations after a fault was applied. This proves the robustness of the DHPEC with fixed parameters (after training) in multi-machine power system as well as SMIB system.

The FACTS device in Fig. 21 could have been placed at a more strategic position, but the best position of a FACTS device is not being studied in this paper.

VI. CONCLUSION

In this paper, the background of the series capacitive reactance compensator (SCRC) was briefly described. Besides describing the *internal* control of the SCRC, the operation of the PI based conventional *external* linear-controller (CONVEC) to improve the damping performance of the SCRC was explained

based on the previous works in [5] and [6], and the study was extended to the CONVEC with two input variables of both active power deviation and speed deviation signals. Then, a new external nonlinear optimal neuro-controller based on the dual heuristic programming algorithm (DHPEC) was designed using the multilayer perceptron neural network (MLPNN).

The simulation results by PSCAD/EMTDC software showed that, when compared to the CONVEC, the DHPEC improves the damping performance for low frequency oscillations at the different operating condition as well as the operating point where the controllers are designed. Moreover, the use of fixed control parameters in the action and critic networks of the DHPEC during real-time operation makes the controllers robust and reduces the requirement of complex computations at each sampling period.

The improved damping of the DHPEC on a single machine infinite bus system has been extended to a multi-machine system.

REFERENCES

- [1] E. W. Kimbark, "Improvement of system stability by switched series capacitors," *IEEE Trans. Power App. Syst.*, vol. PAS-85, pp. 180–188, Feb. 1966.
- [2] N. G. Hingorani and L. Gyugyi, *Understanding FACTS-Concepts and Technology of Flexible AC Transmission Systems*. Piscataway, NJ: IEEE Press, 2000.
- [3] X. Wang, S.-Z. Dai, and B. T. Ooi, "A series capacitive reactance compensator based on voltage source PWM converter," in *Proc. IEEE Ind. Applicat. Soc. Annu. Meeting*, 1991, pp. 918–924.
- [4] B. T. Ooi, S.-Z. Dai, and X. Wang, "Solid-state series capacitive reactance compensators," *IEEE Trans. Power Delivery*, vol. 7, pp. 914–919, Apr. 1990.
- [5] B. S. Rigby and R. G. Harley, "An improved control scheme for a series-capacitive reactance compensator based on a voltage-source inverter," *IEEE Trans. Ind. Applicat.*, vol. 34, pp. 355–363, Mar./Apr. 1998.
- [6] B. S. Rigby, N. S. Chonco, and R. G. Harley, "Analysis of a power oscillation damping scheme using a voltage-source inverter," *IEEE Trans. Industry Applicat.*, vol. 38, pp. 1105–1113, July/Aug. 2002.
- [7] F. J. Swift and H. F. Wang, "Application of the controllable series compensator in damping power system oscillations," *Proc. Inst. Elect. Eng., Gen., Transm. Dist.*, vol. 143, no. 4, pp. 359–364, July 1996.
- [8] J.-W. Park, R. G. Harley, and G. K. Venayagamoorthy, "New internal optimal neurocontrol for a series FACTS device in a power transmission line," *Neural Networks*, vol. 16/5–6, pp. 881–890, July 2003.
- [9] G. K. Venayagamoorthy, R. G. Harley, and D. C. Wunsch, "Dual heuristic programming excitation neurocontrol for generators in a multimachine power system," *IEEE Trans. Ind. Applicat.*, vol. 39, pp. 382–394, Mar./Apr. 2003.
- [10] P. M. Anderson and A. A. Fouad, *Power System Control and Stability*. New York, NY: IEEE Press, 1994.
- [11] *Introduction to PSCAD/EMTDC Version 3.0*.
- [12] J.-W. Park, R. G. Harley, and G. K. Venayagamoorthy, Adaptive critic based optimal neurocontrol for synchronous generator in power system using MLP/RBF neural networks, in *IEEE Trans. Ind. Applicat.*, vol. 39, Sept./Oct. 2003. To appear, Available.
- [13] J.-W. Park, R. G. Harley, and G. K. Venayagamoorthy, On-line identification of synchronous generator: Comparing MLP and RBF neural networks approaches, in *IEEE Trans. Energy Conversion*, 2003. To appear, Available.
- [14] —, "Neuro-identification of a power system equipped with a series capacitive reactance compensator," in *Proc. 35th North Amer. Power Symp.*, Rolla, MO, Oct. 2003, pp. 406–410.
- [15] C. W. Taylor, "Concepts of undervoltage load shedding for voltage stability," *IEEE Trans. Power Delivery*, vol. 7, pp. 480–488, Apr. 1992.
- [16] C. W. Taylor, N. J. Balu, and D. Maratukulam, *Power System Control and Stability*, ser. EPRI Power System Engineering. New York: McGraw-Hill, 1993.
- [17] G. K. Venayagamoorthy, R. G. Harley, and D. C. Wunsch, "Comparison of heuristic dynamic programming and dual heuristic programming adaptive critics for neurocontrol of a turbogenerator," *IEEE Trans. Neural Networks*, vol. 13, pp. 764–773, May 2002.



Jung-Wook Park (S'00–M'03) was born in Seoul, Korea. He received the B.S. degree (Hons.) from the Department of Electrical Engineering at the Yonsei University, Seoul, in 1999, and the M.S.E.C.E. and Ph.D. degrees from the Georgia Institute of Technology, Atlanta, in 2000 and 2003, respectively.

Currently, he is a Research Associate in the Department of Electrical and Computer Engineering at the University of Wisconsin, Madison. His current research interests include power system dynamics, electric machine, flexible ac transmission system (FACTS) device, hybrid system, optimization control algorithms, power quality, and application of artificial neural networks.



Ronald G. Harley (M'77–SM'86–F'92) was born in South Africa. He received the B.Sc.Eng. and M.Sc.Eng. degrees (Hons.) from the University of Pretoria, South Africa, in 1960 and 1965, respectively, and the Ph.D. degree from London University, London, U.K., in 1969.

Currently, he is the Duke Power Company Distinguished Professor at the Georgia Institute of Technology, Atlanta. In 1970, he was appointed to the Chair of Electrical Machines and Power Systems at the University of Natal, Durban, South Africa. His

research interests are in the dynamic and transient behavior of electric machines and power systems, and controlling them by the use of power electronics and intelligent control algorithms.

Dr. Harley is a Fellow of the SAIEE, a Fellow of the IEE, and a Fellow of the IEEE. He is also a Fellow of the Royal Society in South Africa, a Fellow of the University of Natal, and a Founder Member of the Academy of Science in South Africa formed in 1994. He was elected as a Distinguished Lecturer by the IEEE Industry Applications Society for the years 2000–2001. In 2003–2004, he is serving as the Vice-President (Operations) of IEEE Power Electronics Society.



Ganesh Kumar Venayagamoorthy (S'91–M'97–SM'02) was born in Jaffna, Sri Lanka. He received the B.Eng. (Hons.) degree with a first class in electrical and electronics engineering from the Abubakar Tafawa Balewa University, Bauchi, Nigeria, in 1994, and the M.Sc.Eng. and Ph.D. degrees in electrical engineering from the University of Natal, Durban, South Africa, in 1999 and 2002, respectively.

Currently, he is an Assistant Professor at the University of Missouri, Rolla. He was appointed Lecturer at the Durban Institute of Technology, South Africa, from 1996 to 2001, and Senior Lecturer from 2001 to 2002. He was a Research Associate at Texas Tech University, Lubbock, in 1999, and at the University of Missouri, Rolla, in 2000/2001. His research interests include power systems, control systems, computational intelligence, and evolving hardware.

Dr. Venayagamoorthy is a 2001 recipient of the IEEE Neural Network Society summer research scholarship and the 2003 International Neural Network Society Young Investigator award recipient. He is a member of South African Institute of Electrical Engineers.